

Liouville partial-differential-equation methods for computing 2D complex multivalued eikonals in attenuating media

Shingyu Leung¹, Jiangtao Hu², and Jianliang Qian³

ABSTRACT

We have developed a Liouville partial-differential-equation (PDE)-based method for computing complex-valued eikonals in real phase space in the multivalued sense in attenuating media with frequency-independent qualify factors, where the new method computes the real and imaginary parts of the complex-valued eikonal in two steps by solving Liouville equations in real phase space. Because the earth is composed of attenuating materials, seismic waves usually attenuate so that seismic data processing calls for properly treating the resulting energy losses and phase distortions of wave propagation. In the regime of high-frequency asymptotics, the complex-valued eikonal is one essential ingredient for describing wave propagation in attenuating media because this unique quantity summarizes two wave properties into one function: Its real part describes the wave kinematics and its imaginary part captures the effects of phase dispersion and amplitude attenuation. Because some popular ordinary-differential-equation (ODE)-based ray-tracing methods for computing complex-valued eikonals in real space distribute the eikonal function irregularly in real space, we are motivated to develop PDE-based Eulerian methods for computing such complex-valued eikonals in real space on regular meshes. Therefore, we solved novel paraxial Liouville PDEs in real phase space so that we can compute the real and imaginary parts of the complex-valued eikonal in the multivalued sense on regular meshes. We call the resulting method the Liouville PDE method for complex-valued multivalued eikonals in attenuating media; moreover, this new method provides a unified framework for Eulerianizing several popular approximate real-space ray-tracing methods for complex-valued eikonals, such as viscoacoustic ray tracing, real viscoelastic ray tracing, and real elastic ray tracing. In addition, we also provide Liouville PDE formulations for computing multivalued ray amplitudes in a weakly viscoacoustic medium. Numerical examples, including a synthetic gas-cloud model, demonstrate that our methods yield highly accurate complex-valued eikonals in the multivalued sense.

INTRODUCTION

Because the earth is composed of porous and granular subsurface rocks, seismic wave propagation is intrinsically attenuating (Červený et al., 1977; Aki and Richards, 1980; Carcione, 2015); this calls for properly treating attenuation effects in seismic data processing so as to delineate geologic structures reliably. Consequently, it is crucial to develop efficient modeling methods for wave propagation in attenuating media. Although direct modeling methods such as finite-difference and finite-element methods are abundant (Robertsson et al.,

1994; Blanch et al., 1995; Blanch and Robertsson, 1997; Carcione, 1999, 2009; Carcione et al., 2002; Zhang et al., 2010; Xie et al., 2015), we seek alternative modeling methods using high-frequency asymptotics (Červený et al., 1977; Gajewski and Pšenčik, 1992; Hanyga and Seredyňska, 2000; Keers et al., 2001; Vavryčuk, 2008a; Hao and Alkhalifah, 2017; Huang and Greenhalgh, 2018; Huang et al., 2018). Such methods have some unique merits; for example, they yield quantities that can be easily incorporated into existing migration, inversion, or tomography codes. To develop an asymptotic method for waves in attenuating media, we apply the asymptotic

Manuscript received by the Editor 12 February 2021; revised manuscript received 29 August 2021; published ahead of production 2 November 2021; published online 30 December 2021.

Hong Kong University of Science and Technology, Department of Mathematics, Hong Kong SAR 999077, China. E-mail: masyleung@ust.hk

²State Key Laboratory of Oil and Gas Reservoir Geology and Exploitation (Chengdu University of Technology), Key Laboratory of Earth Exploration and Information Techniques (Chengdu University of Technology), Ministry of Education, Dongsanlu, Erxianqiao, Chengdu 610059, China. E-mail: jiangtao_hu@ 126.com (corresponding author)

³Michigan State University, Department of Mathematics and Department of CMSE, East Lansing, Michigan 48824, USA. E-mail: jqian@msu.edu (corresponding author).

© 2022 Society of Exploration Geophysicists. All rights reserved

T72 Leung et al.

method to the viscoelastic isotropic wave equation with frequencydependent complex-valued elastic parameters defined in complex space, leading to the complex-valued P- and S-wave eikonal equations defined in complex space (in the sense that its variables are in complex space). Because the imaginary part of the complex-valued eikonal captures phase dispersion and amplitude attenuation, the complex-valued eikonal is a unique quantity, which can be useful for efficient seismic data processing. This raises the question of how to compute such complex-valued eikonals efficiently. In this paper, we develop novel paraxial Liouville partial-differential-equation (PDE) methods in real phase space so that we can compute a complex-valued eikonal in real space (in the sense that its variables are in real space) in the multivalued sense on regular meshes. We develop the new methodology by reformulating some popular real-space ordinary-differential-equation (ODE)-based Lagrangian ray-tracing methods for complex-valued eikonals into PDE-based methods, in which the real and imaginary parts of the complex-valued eikonal have real-space variables and are computed separately by solving some linear Liouville equations.

To facilitate the development of our methodology, we first clarify some notions and concepts. Although traveltime and eikonal are treated the same in many situations of nonattenuating wave propagation, we will distinguish them carefully in our discussion for the following reasons: The real and imaginary parts of the eikonal are well defined in attenuating wave propagation, and the traveltime function itself in attenuating wave motion depends on complex-valued eikonal and frequency (for an example, see Keers et al., 2001). By real space in our discussion, we mean 2D or 3D physical space. By complex space, we mean that each real coordinate becomes complex-valued, including real and imaginary parts, so that 2D real space becomes 2D complex space; the latter, in fact, is four dimensions in the sense of having two real coordinates associated with two real parts and two real coordinates associated with two imaginary parts. Moreover, a complex-valued eikonal can be defined in either complex or real space in the sense that its real and imaginary parts have variables in either complex or real space. In the sequel, a complex-valued eikonal is mainly meant to indicate that its real and imaginary parts have variables in real (phase) space.

According to classical mechanics (Goldstein, 1950), we use real phase space to denote the space spanned by real position and real momentum variables, which are used to describe the motions of particles according to Newton's laws. Thus, in 2D real space, the corresponding real phase space is four dimensions, consisting of two real position variables and two real momentum variables. However, in our application here related to the eikonal equation in 2D real space, the eikonal equation itself serves as a constraint to constrain real momentum variables so that one real phase angle is sufficient to characterize the two real momentum variables; consequently, we have a reduced real phase space of three dimensions composed of two real position variables and one real phase angle. Accordingly, for the 3D real-space eikonal equations, the corresponding real phase space is six dimensions but the reduced real phase space is five dimensions. We may generalize real phase space to complex phase space naturally by replacing real space with complex space in the context of real phase space.

As a first-order nonlinear PDE, the complex-valued eikonal equation defined in complex space can be solved by the method of characteristics to yield complex-valued eikonal functions, leading to the so-called complex-space ray-tracing method, which theoretically

enables us to solve the complex-valued eikonal equation without any approximation. However, because sources and receivers in the seismic acquisition geometry are located in real (physical) space, the complex-space ray-tracing method brings about unusual complications in that rays are now situated in complex space so that the dimension of the ambient space becomes doubled, where a usual 2D real-space ray tracing becomes a 2D complex-space (equivalent to a 4D real space) ray tracing; consequently, the resulting ray-tracing system is high dimensional and relatively costly to solve. Moreover, it is hard to build a complex-valued elastic-parameter model from the real-valued one, which is usually available from measurements in real space (Vavryčuk, 2008a; Hao and Alkhalifah, 2017). Therefore, some further approximations are required to develop real-space ray-tracing methods for computing complex-valued eikonal functions.

In viscoacoustic media, the widely used weakly attenuating approximation (i.e., the reciprocal of frequency-independent quality factor ≪ 1; Červený et al., 1977; Gajewski and Pšenčik, 1992; Keers et al., 2001; Xie et al., 2009; Xin et al., 2014; Hu et al., 2018) can be used to reduce the complex-space ray-tracing system to a real-space ray-tracing system approximately in terms of quality factors, where the real and imaginary parts of the complex-valued eikonal are defined in real space. Numerical experiments in Gajewski and Pšenčik (1992) demonstrated that the weakly attenuating assumption is applicable to a substantial range of quality factors encountered in exploration geophysics. Keers et al. (2001) show that the raypath under the weakly attenuating approximation is identical to that in a corresponding nonattenuating medium defined by a real-valued reference velocity; therefore, the real part of the complex-valued eikonal can be obtained by applying the ray-tracing method to the eikonal equation defined by the real-valued reference velocity, and the imaginary part can be obtained via an integration along the known raypath defined by the reference velocity. In this approximate real-space ray-tracing model, the real and imaginary parts of the complex-valued eikonal at each location must be found indirectly via solving nonlinear systems or numerical quadratures.

Viewing a viscoelastic medium as the perturbation of a perfectly elastic medium, one may account for attenuation effects by using first-order perturbations and tracing rays in the elastic reference medium which is specified in real space (Vavryčuk, 2008b; Klimeš and Klimeš, 2011; Hao and Alkhalifah, 2017; Li et al., 2020), leading to the real-elastic ray-tracing method (Vavryčuk, 2012). Another real-space ray-tracing method for viscoelastic media, the real viscoelastic ray-tracing method (Vavryčuk, 2008a), is obtained by modifying the Hamiltonians for viscoelastic media so that the rays are constrained as trajectories in real space (Vavryčuk, 2012). The resulting ray-tracing system is based on a certain real-valued reference velocity calculated from the complex-valued phase velocity for the P- or S-wave, respectively. Although this approach is still approximate, this method is highly accurate and applicable to strongly attenuating media (Vavryčuk, 2012; Hao and Alkhalifah, 2017), where the real and imaginary parts of the complex-valued eikonal are obtained in the same way as in the real elastic ray-tracing method.

So far, because all the rays are traced from an arbitrary source point to subsurface locations by solving an initial value problem for ODEs, all these real-space ray-tracing methods yield the real and imaginary parts of the complex-valued eikonal at irregularly distributed points. Such methods, which track individual particles (pulses of seismic energy) through space along raypaths, are called Lagrangian. Because irregular distributions of complex-valued eikonals hinder their applications to seismic migration and tomography as these applications are usually posed on regular mesh points, we are motivated to develop efficient methods to produce complexvalued eikonals on regular grids; we do this by formulating the three real-space ray-tracing systems into partial differential equations. It turns out that there are two possibilities for this.

Assuming that there is a unique ray connecting any source to any grid point, one possibility is to solve an eikonal equation with an appropriate reference velocity for the real part of the complex-valued eikonal and solve an "advection equation" with an appropriate quality-factor function as its forcing term for the imaginary part of the complex-valued eikonal, where the advection equation is weakly coupled to the eikonal equation in the sense that the advection coefficients are defined by the gradient of the real part of the complexvalued eikonal; the resulting method yields a single-valued approximate solution for the complex-valued eikonal equation. Such methods, which track the movement of "particles" through a fixed point in real space, produce a field of one or more quantities at each fixed point, are called Eulerian. Because the unique-ray assumption is very restrictive, we would in fact solve the preceding eikonal equation for the real part in the sense of viscosity solution (Lions, 1982; van Trier and Symes, 1991), ending up by computing the first-arrival-based real part of the complex-valued eikonal. This route has been taken in the recent work of Hu et al. (2021).

However, assuming that there may be multiple rays connecting any source to any grid point, the other possibility is to embed the real-space ray-tracing system into real phase space Liouville equations (tracking the movement of particles through a fixed point in real phase space) and solve the resulting linear PDEs in real phase space so as to obtain the real and imaginary parts of the complex multivalued eikonal on regular mesh points in physical space. The resulting Eulerian method yields multivalued real and imaginary parts of the complex-valued eikonal, and we call this Eulerian method the Liouville PDE method. This is the route that we are taking in the current work to develop Eulerian methods for computing complex-valued eikonals in real space.

If the medium is heterogeneous, there is a high probability that more than one ray will occupy any given spatial point, resulting in a multivalued eikonal field over physical space (White, 1984). Nevertheless, the multivalued eikonal field is essential, for example, in obtaining high-resolution seismic images by multiarrival Kirchhoff and Gaussian beam migrations (Liu and Bleistein, 1995; Operto et al., 2000; Hill, 2001; Gray, 2005) and by ray-based Q-migrations (Xie et al., 2009, 2015). The Lagrangian approach to this problem is to use the method of characteristics to trace rays in phase space, thus taking care of multivaluedness (Červený et al., 1977; Pereyra, 1992). However, because in reality only a finite number of rays can be traced, Lagrangian methods in general produce nonuniform distributions of the eikonal field. The solution to this nonuniformity is interpolation, which can be cumbersome (Pereyra, 1992; Vinje et al., 1993). Therefore, Eulerian approaches are highly desirable for solving eikonal equations and, consequently, much research has been devoted to this. Benamou (1999) enacts direct resolution of multivalued phase space solutions of Hamilton-Jacobi equations. Symes (1998) and Symes and Qian (2003) derive a slowness matching finite-difference method for computing multivalued eikonals by patching together local single-valued solutions of the eikonal equation via Fermat's principle into a global multivalued traveltime field. Engquist et al. (2002) use the segment projection method to reparameterize multivalued wavefronts into single-valued segments existing in a different space. Fomel and Sethian (2002) introduce a phase space stationary Liouville equation method that yields multivalued eikonals for multiple sources when they occur. Osher et al. (2002) introduce a phase space-based level set and Eulerian framework for constructing wavefronts, which automatically handles multivalued solutions when they appear. Qian et al. (2003) extend the level-set method (Osher et al., 2002) to anisotropic wave propagation. Qian and Leung (2004, 2006) extend the level-set method (Osher et al., 2002) to the paraxial Liouville setting so that multivalued eikonals and amplitudes can be computed efficiently, and this paraxial Liouville formulation is adopted in the current work.

Our contribution consists of the following. We first formulate the paraxial Liouville equations for computing the real part of the complex-valued eikonal in real reduced phase space, and we then derive a new paraxial Liouville equation for computing the imaginary part of the complex-valued eikonal in real reduced phase space. The imaginary part of the complex-valued eikonal determines phase dispersion and amplitude attenuation. We also formulate the paraxial Liouville equations to compute multivalued ray amplitudes in real reduced phase space. To have an efficient algorithm, we also develop a fast local level-set method to compute these multivalued functions rapidly in real reduced phase space.

The rest of the paper is organized as follows. In the Methodology section, we develop the paraxial Liouville formulation to compute the real and imaginary parts of the complex-valued eikonal, and we also derive necessary equations for computing amplitudes. Then, numerical experiments on typical attenuating models demonstrate the feasibility of the proposed method.

METHODOLOGY

Eulerian PDE framework for complex-valued eikonals: Single arrivals

In this subsection, we briefly summarize the approach in Hu et al. (2021) for computing complex-valued eikonals defined in real space in attenuating media, where the real part of the complex-valued eikonal is the first arrival of the isotropic eikonal equation in the sense of viscosity solution. The correspondence principle (Keers et al., 2001) indicates that we can treat wave propagation in a viscoelastic (or viscoacoustic) medium as wave propagation through an elastic (or acoustic) medium with complex-valued elastic parameters in complex space (or a complex-valued velocity in complex space). To model wave motion in such a medium efficiently, highfrequency asymptotic approximations provide an effective alternative to direct numerical methods. One of the essential ingredients for high-frequency asymptotics of viscous wave motion is the complexvalued eikonal function. Hu et al. (2021) propose a unified Eulerian framework to compute complex-valued eikonal functions in real space for several popular high-frequency asymptotic models of viscous wave motions, where the real and imaginary parts of the complex-valued eikonal function satisfy the real-space isotropic eikonal equation and a real-space advection equation, respectively. These popular asymptotic methods include the real-space ray-tracing method (Gajewski and Pšenčik, 1992; Keers et al., 2001) for viscoacoustic media, the real-elastic ray-tracing method (Vavryčuk, T74 Leung et al.

2008b, 2012; Klimeš and Klimeš, 2011; Hao and Alkhalifah, 2017), and the real viscoelastic ray-tracing method (Vavryčuk, 2008a, 2012; Hao and Alkhalifah, 2017) for viscoelastic media. Provided that we choose an appropriate *reference velocity* and an appropriate quality-factor related function, the framework in Hu et al. (2021) is applicable to compute complex-valued eikonals in weakly and strongly attenuating media.

Hu et al. (2021) focus on developing PDE-based methods in the sense of first arrivals, and in the current work we are going to develop PDE-based methods in the sense of multivalued solutions (multiple arrivals). We start from Hu et al. (2021) to develop such an approach for computing multivalued real and imaginary parts of the complex-valued eikonal.

We assume that the complex-valued eikonal function τ consists of the real part T and the imaginary part T^* , which satisfy the following real-space eikonal and advection equation (Hu et al., 2021), respectively,

$$|\nabla T| = \frac{1}{c(\mathbf{x})}, \quad T(\mathbf{x}_s) = 0, \tag{1}$$

$$\nabla T \cdot \nabla T^* = \frac{1}{c^2(\mathbf{x})Q(\mathbf{x})}, \quad T^*(\mathbf{x}_s) = 0, \tag{2}$$

where \mathbf{x} is the real-valued position vector, $c(\mathbf{x})$ is the real-valued reference velocity, and $Q(\mathbf{x})$ is a quality-factor-related real-valued function (and is not necessarily the frequency-independent quality factor itself).

Because ∇T is parallel to the ray direction, the imaginary part T^* actually satisfies

$$T^*(\mathbf{x}) = \int_{R(\mathbf{x})} \frac{1}{c(\mathbf{y}(s))Q(\mathbf{y}(s))} ds,$$
 (3)

where the integration is over the raypath $R(\mathbf{x})$ connecting the source \mathbf{x}_s to the point \mathbf{x} , and the coordinate function $\mathbf{y}(s)$ varies along the raypath $R(\mathbf{x})$ parameterized by the arc length s.

Hu et al. (2021) develop high-order fast sweeping methods to solve equations 1 and 2, and the resulting real part of the complex-valued eikonal is understood as the minimum phase or the first-arrival traveltime in the viscosity-solution sense for Hamilton-Jacobi equations (Lions, 1982; van Trier and Symes, 1991). However, because the single-valued Eulerian solution may not suffice for many applications, it motivates us to develop efficient Eulerian methods for computing the complex-valued eikonal in the multivalued sense.

A paraxial Liouville formulation for complex-valued eikonals: Multivalued

To simplify the derivation, we consider the 2D case so that we have $\mathbf{x} = (x, z)$; a similar derivation can be carried out in the 3D case (Leung et al., 2004). We follow the work in Qian and Leung (2004, 2006) to develop a simple numerical approach so that we can compute the multivalued real part of the complex-valued eikonal by using the level-set method and the paraxial formulation for the eikonal equation 1. We assume that the eikonals of interest are carried by the so-called subhorizontal rays (Gray and May, 1994; Symes, 1998; Qian and Symes, 2002), where subhorizontal means oriented in the positive z-direction.

Applying the method of characteristics to the eikonal equation 1 with the point source condition under the subhorizontal condition, we can use depth z as the running parameter so that we have the following reduced system (Qian and Leung, 2004, 2006):

$$\frac{dx}{dz} = \tan \theta,\tag{4}$$

$$\frac{d\theta}{dz} = \frac{1}{c} \left(\frac{\partial c}{\partial z} \tan \theta - \frac{\partial c}{\partial x} \right),\tag{5}$$

which is appended with the initial conditions $x|_{z=0} = x_s$ and $\theta|_{z=0} = \theta_s$. Here, θ_s varies from $-\theta_{\max} \le \theta \le \theta_{\max} < (\pi/2)$. In addition, the eikonal itself is computed by integrating

$$\frac{dt}{dz} = \frac{1}{c\cos\theta},\tag{6}$$

with $t|_{z=0} = 0$.

To develop Eulerian methods, we will use the level-set-based Liouville equations. If we define $\phi = \phi(z, x, \theta)$ such that the zero level set, $\{(x(z), \theta(z)) : \phi(z, x(z), \theta(z)) = 0\}$, gives the location of the reduced bicharacteristic strip $(x(z), \theta(z))$ at the "artificial time" z, then we may differentiate the zero level set equation with respect to z to obtain (Qian and Leung, 2004, 2006)

$$\phi_z + u\phi_x + v\phi_\theta = 0, (7)$$

where u = dx/dz and $v = d\theta/dz$ are given by the ray equations 4 and 5. The initial condition for the level set equation 7 is taken to be $\phi|_{z=0} = \phi(0, x, \theta) = x - x_s$, which implies that the zero level is set at z = 0 and

$$\begin{cases}
(x(0), \theta(0)) : \phi(0, x(0), \theta(0)) = 0 \\
= \{(x(0), \theta(0)) : x(0) - x_s = 0 \\
= \{(x(0), \theta(0)) : x(0) = x_s \},
\end{cases} (8)$$

parameterizes all the rays emanating from the source $(x_s, z = 0)$ with the takeoff angle ranging from $-\theta_{\text{max}} \le \theta \le \theta_{\text{max}} < (\pi/2)$.

To determine the multivalued real part of the complex-valued eikonal from the previous level-set equation, we give the corresponding equation governing the evolution of the real part. By the subhorizontal condition in the paraxial formulation and the ray equation 6, let $F_{\mathbf{u}}(x,\theta;z)$ be the flow generated by the vector field $\mathbf{u}=(u,v)$ in the reduced phase space (x,z,θ) along the z-direction. Thus, we can write

$$\frac{dT}{dz}(z, F_{\mathbf{u}}(x, \theta; z)) = \frac{1}{c \cos \theta}.$$
 (9)

Therefore, having $t = T(z, x, \theta)$ we get the following advection equation (Qian and Leung, 2004, 2006):

$$\frac{dT}{dz} = T_z + uT_x + vT_\theta = \frac{1}{c\cos\theta}.$$
 (10)

The initial condition for T is given by $T|_{z=0} = T(0, x, \theta) = 0$.

The imaginary part of the complex-valued eikonal can be computed by converting the Lagrangian (ray-tracing) formulation to

the corresponding Eulerian (PDE) formulation. According to the ray-theory solution in equation 3, we can write

$$\frac{dT^*}{dz}(z, F_{\mathbf{u}}(x, \theta; z)) = \frac{1}{cO\cos\theta},\tag{11}$$

where $F_{\mathbf{u}}(x,\theta;z)$ is the same flow generated by the vector field **u** in the reduced phase space. This implies that the imaginary part of the eikonal, T^* , satisfies the following equation:

$$\frac{dT^*}{dz} = T_z^* + uT_x^* + vT_\theta^* = \frac{1}{cQ\cos\theta},$$
 (12)

which is a new equation that will enable us to compute the multivalued imaginary part of the complex-valued eikonal in a PDE fashion.

A paraxial Liouville formulation for multivalued amplitudes

According to Keers et al. (2001), when the quality factor satisfies $(1/O) \ll 1$ in a viscoacoustic medium, then, to the first order, the raypaths remain unchanged and the amplitude also is unchanged, and furthermore they can be determined from the reference acoustic velocity. In practice, the assumption $(1/Q) \ll 1$ may be overly restrictive, and we found in our experiments that the method still works when (1/Q) < 1. However, in a generic viscoelastic medium, it is unknown whether the P- or S-wave amplitude is unchanged to the first order in terms of the quality factor. Therefore, we will develop our paraxial Liouville formulation for multivalued amplitudes only in a weakly viscoacoustic medium.

Consequently, in the sense of Keers et al. (2001), based on the same paraxial Liouville framework, we can compute the multivalued amplitude corresponding to the multivalued real part of the eikonal, so that the multivalued amplitude is real valued rather than complex valued. We start from the level-set approach as developed by Qian and Leung (2004, 2006) and the formula given in Zhang (1993) and Qian and Symes (2002),

$$\tilde{A}(x,z;x_s,z_s) = \frac{1}{2\pi} \sqrt{\frac{c}{2}} \sqrt{|\nabla \tilde{T} \times \nabla \tilde{\psi}|}, \qquad (13)$$

where \tilde{T} and $\tilde{\psi}$ are the real part of the eikonal and the take-off angle of a *unique* real-space ray reaching (x, z) from (x_s, z_s) , respectively. When the real-space ray connecting the source (x_s, z_s) to the subsurface point (x, z) is not unique, the amplitude function becomes multivalued, where the real part of the complex-valued eikonal and the takeoff angle are well defined on each solution branch in physical space (x, z).

To compute the multivalued amplitude function in the reduced phase space, we consider T as the extension of real-space \tilde{T} to the reduced phase space; furthermore, we also may extend $\tilde{\psi}$ and A to ψ and A in the (z, x, θ) space, respectively. Because the takeoff angle is constant along a given ray in phase space, we have (Qian and Leung, 2004, 2006)

$$\psi_z + u\psi_x + v\psi_\theta = 0. \tag{14}$$

Although the takeoff angle and the level-set function satisfy the same advection equation, the initial conditions for the two advection equations are different, so that the two equations propagate different information. The level-set function is initialized to be $\phi(z=0,x,\theta)=$ $x - x_s$ so that the zero level set $\{(x^*, \theta^*): \phi(z, x^*, \theta^*) = 0\}$ at a certain quasi-time z indicates that a ray emanating from the source x_s at z=0 passes through the point (x^*,z) with the arrival angle θ^* . The takeoff-angle function ψ is initialized to be $\psi(z=0,x,\theta)=\theta$ so that the value of $\psi(z, x, \theta)$ at (z, x, θ) indicates that a ray with the takeoff angle equal to $\psi(z, x, \theta)$ has arrived at the location (z, x) with the arrival angle θ . Combining the two pieces of information from the level-set function and the takeoff angle function, we can read off the source and takeoff angle of the ray arriving at the location (z, x^*, θ^*) , where the takeoff angle and the source of the ray are equal to $\psi(z, x^*, \theta^*)$ and x_s , respectively.

The work in Qian and Leung (2006) has shown that the amplitude formula can be reduced to

$$A(z; x, \theta) = \frac{1}{2\pi} \sqrt{\frac{c}{2 \cos \theta}} \sqrt{\left| \frac{\psi_x \phi_\theta - \psi_\theta \phi_x}{\phi_\theta} \right|}.$$
 (15)

To compute the derivatives of the level-set function on the zero level set, we need to advect those derivatives as well. We first let $\xi = \phi_x$ and $\eta = \phi_\theta$. Differentiating the advection equation for ϕ with respect to x and θ , respectively, we have (Qian and Leung, 2004, 2006)

$$\xi_{z} + u\xi_{x} + v\xi_{\theta} + u_{x}\xi + v_{x}\eta = 0, \tag{16}$$

$$\eta_z + u\eta_x + v\eta_\theta + u_\theta \xi + v_\theta \eta = 0. \tag{17}$$

Now, defining $\Delta = \psi_x \phi_\theta - \psi_\theta \phi_x$ and differentiating it with respect to z, we have the advection equation (Oian and Leung, 2004, 2006):

$$\Delta_z + \nabla_{x,\theta} \cdot (\mathbf{u}\Delta) = 0, \tag{18}$$

and the amplitude can then be computed by

$$A(z; x, \theta) = \frac{1}{2\pi} \sqrt{\left| \frac{c}{2 \cos \theta} \frac{\Delta}{\phi_{\theta}} \right|}.$$
 (19)

We remark that the quantity Δ is inversely proportional to the crosssectional area of an infinitesimal tube of rays surrounding a certain given ray and is conserved along the flow defined by the vector field **u**. The scaling factor $1/(2 \cos \theta)$ is related to the paraxial perspective of the reduced phase space in the z-direction.

Now, we consider the initial conditions for these intermediate quantities in the multivalued amplitude formula. At z = 0, we can set ϕ_x and ϕ_θ equal to 1 and 0, respectively. However, because ψ_x is a singular function at the source, it is better to start computing ψ_x and ψ_θ at some z = dz > 0 close to zero. Assuming that the velocity c can be approximated by a constant near the source, we have (Qian and Leung, 2004, 2006)

$$|\psi_x(z, x, \theta)|_{z=dz} = \frac{\cos^2 \theta}{dz}, \quad |\psi_\theta(z, x, \theta)|_{z=dz} = 1.$$
 (20)

Thus at small z = dz > 0, we assign $\phi(z, x, \theta)|_{z=dz} = x - dz \tan \theta$ and $\Delta(dz, x, \theta) \equiv -2$, which is independent of dz as long as the velocity can be well approximated by a constant near the source.

T76 Leung et al.

Numerical implementations

There are well-developed numerical algorithms and packages for solving these PDEs numerically. In this work, we apply the fifth-order weighted essentially nonoscillatory-Godunov scheme (Jiang and Peng, 2000) for approximating spatial derivatives and use a third-order total-variation diminishing-Runge-Kutta method (Osher and Shu, 1991) for time stepping. One also might consider the flow-map-based methods developed in You et al. (2017) and You and Leung (2018, 2020).

To speed up the overall computation of the algorithm, we propose incorporating the local level-set framework (Peng et al., 1999; Qian and Leung, 2006) into the algorithm. Because we are only interested in the zero level set, all the updates can actually be done in a tube centered at $\phi = 0$. Therefore, by considering only the grid points within this tube, the complexity of the entire algorithm can be reduced by a factor of N from $O(N^3LogN)$ to $O(N^2LogN)$, where N is the number of grid points in each physical dimension.

NUMERICAL EXPERIMENTS

In the examples, we consider the following two Q models given by

$$Q_1(x,z) = 100 - 50 \exp\left[-\frac{(x-x_0)^2 + (z-z_0)^2}{2\sigma^2}\right],$$
 (21)

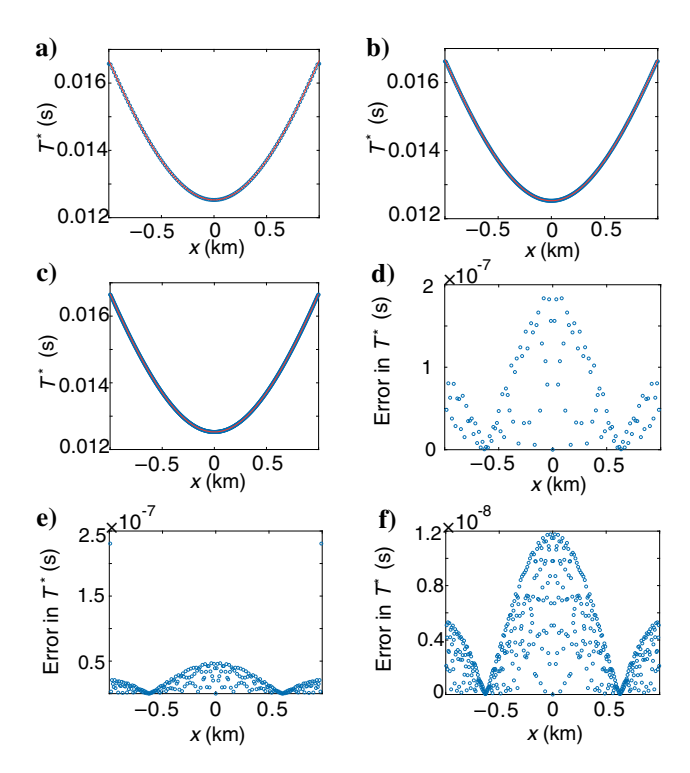


Figure 1. Constant velocity model with $Q=Q_1$. The computed imaginary part of the eikonal at z=1.0 km using a mesh of (a) 121×121 , (b) 241×241 , and (c) 481×481 . The exact imaginary part of the eikonal is plotted using a solid red line. The corresponding absolute errors for different meshes are shown in (d-f), respectively.

$$Q_2(x, z) = 10000 - 995011_{\mathcal{B}_{0.2}(0, 0.5)}(x, z)$$

$$= \begin{cases} 50 & \text{if } (x, z) \in \mathcal{B}_{0.2}(0, 0.5), \\ 10000 & \text{otherwise} \end{cases}$$
(22)

where $(x_0, z_0) = (0.5, 0)$ km, $\sigma = 0.25$, $\mathcal{B}_{0.2}(0, 0.5)$ represents the disk centered at (0, 0.5) km with radius 0.2 km, and 1_{Ω} is the characteristic function of the set Ω .

Constant velocity model

We take the reference velocity to be $c(x,z) \equiv 1$ km/s and the domain to be $[-1,1] \times [0,1]$ km. We first consider the smooth model $Q=Q_1$. Figure 1 shows the imaginary part of the complex-valued eikonal at the final level z=1 km computed using different meshes. We observe that the computed imaginary part at the center point (x,z)=(0,1) km is accurate up to machine epsilon. The L_1 and L_2 errors in the solution

$$E_1 = \sum |T_i^* - T_i^{\text{exact}}| \Delta x \text{ and } E_2 = \left[\sum (T_i^* - T_i^{\text{exact}})^2 \Delta x\right]^{\frac{1}{2}}$$
(23)

are shown in Table 1, where i enumerates the mesh points. It demonstrates a clean second-order convergence of the computed imaginary part.

We also have carried out an experiment with the discontinuous model $Q=Q_2$. The computed imaginary part of the eikonal and the related absolute errors are plotted in Figure 2. As shown in Table 2, the computed solution shows the second-order convergence in the order of $O(\Delta x^2)$ at the point (x,z)=(0,1) km. When we look at the L_1 or L_2 errors in the computed imaginary part, however, the discretization error of the discontinuous Q model makes the accuracy of the computed imaginary part degraded significantly so that the rate of convergence is dropped to the first order.

Waveguide model

The computational domain is $[-1, 1] \times [0, 2]$ km. The reference velocity function (km/s) is given by

$$c(x, z) = 1.1 - \exp(-0.5x^2),$$
 (24)

which is symmetric with respect to x = 0 km. Because we have the same symmetry in Q, we expect the same type of symmetry

Table 1. Constant velocity model with $Q = Q_1$.

	L_1	Rate	L_2	Rate	
121	1.234e-7	_	1.235e-7	_	
241	3.484e-8	1.824	4.114e-8	1.464	
481	7.852e-9	2.149	7.141e-9	2.526	

The L_1 and L_2 errors in the imaginary part of the complex-valued eikonal at z=1 km.

in the real and imaginary parts of the complex-valued eikonal and the real-valued amplitude.

Figure 3 shows the computed real and imaginary parts of the complex-valued eikonal at z = 0.48, 0.96, and 1.6 km, where different arrivals are plotted using different colors. The first row in Figure 3 shows the real part of the eikonal, which is solely determined by the given reference velocity. The second row shows the imaginary part of the eikonal at different depths corresponding to the smooth Q model, $Q = Q_1$. Although most rays from the source will curve, the one with the zero initial takeoff angle will not curve so that a reference solution for that particular ray can be computed by integrating $\int_0^{z_f} dz/cQ$. We observe that this ray corresponds to the latest arrival ray, i.e., the third arrival, to the point $(x, z) = (0, z_f)$ km. The numerical errors at this particular point based on different meshes, 121 × 121, 241 × 241, and 481×481 , are all of machine epsilon, i.e., $O(10^{-16})$. This is

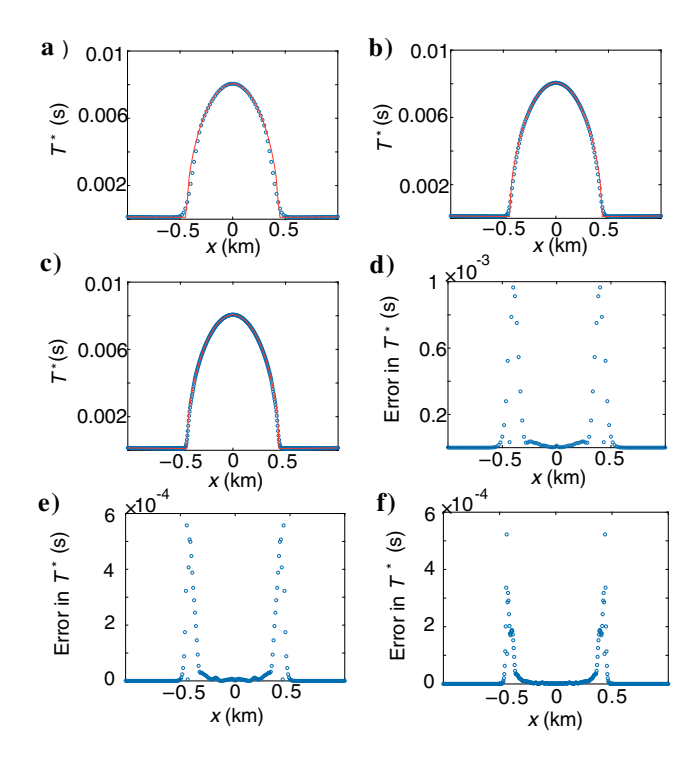


Figure 2. Constant velocity model with $Q = Q_2$. The computed imaginary part of the eikonal at z = 1.0 km using a mesh of (a) 121×121 , (b) 241×241 , and (c) 481×481 . The exact imaginary part of the eikonal is plotted using a solid red line. The corresponding absolute errors for different meshed are shown in (d-f), respectively.

consistent with the conclusion from the constant case. The third row shows the imaginary part of the eikonal at different depths corresponding to the discontinuous Q model, $Q = Q_2$, where the errors at that particular point are significantly increased to $O(10^{-5})$. Figure 4 compares our numerical solutions with the solutions computed by the ray-tracing method. We partition the θ -domain uniformly so that the initial takeoff angle is evenly distributed from $-9\pi/20$ to $9\pi/20$. We plot the PDE solutions using blue dots and plot the ray-tracing solutions using red circles. As we can see because there is no control of where the arrival locations will be, the real and imaginary parts of the complex-valued eikonal from the ray-tracing method cannot be uniformly sampled on the x-axis, which is in sharp contrast to our PDE approach.

Figure 5 shows the imaginary part of the eikonal, ϕ_{θ} , Δ and also the amplitude at z = 1.6 km computed on the 481 \times 481 grid, where the Q model $Q = Q_1$. Because this particular velocity model satisfies $u_x = v_\theta = 0$, the equation for Δ is purely advective. This implies that Δ is analytically given by -2 everywhere. We see that the computed Δ matches with this exact solution very well. Because ϕ_{θ} approaches 0 as we approach the caustics near $x = \pm 0.45$ km, the amplitude function becomes infinite at these locations.

Sinusoidal model

This example is adapted from the sinusoidal model used in Symes (1998) and Symes and Qian (2003), where the velocity function (km/s) is given by

$$c(x, z) = 1 + 0.2 \sin(0.5\pi z) \sin[3\pi(x + 0.55)], \qquad (25)$$

where the computational domain is $[-1, 1] \times [0, 2]$ km.

Figure 6 shows the velocity model, and the total number of grid points is 241×241 . The model dimension is 2 km in the x- and z-directions. A particular feature of this model is that high and low velocity regions alternate laterally. When seismic rays pass through these areas, the rays will bend so that they will converge or diverge alternately. Figure 6 also shows that the rays emanating from the source at (x, z) = (0, 0)km are overlaid on the velocity model. There are 181 rays, where the takeoff angle is sampled uniformly in the interval $[-\pi/2, \pi/2]$. The figure also demonstrates two unique features of this model. First, the diverging rays create large shadow zones where it is challenging to obtain reliable eikonal information. Second, the converging rays make the real part of the complex-valued eikonal multivalued so that it is challenging for conventional first-arrival traveltime computational methods to capture all the useful eikonal information.

Figure 7 shows the multivalued real part of the complex-valued eikonal at z = 0.6, 1.2, and 2.0 km. As z evolves, we see that a

Table 2. Constant velocity model with $Q = Q_2$.

	Error at (0, 1.0) km	Rate	L_1 at $z = 1$ km	Rate	L_2 at $z = 1$ km	Rate
121 × 121	1.208e-5	_	1.986e-4	_	3.549e-4	_
241×241	2.780e-6	2.1097	8.725e-5	1.1865	1.738e-4	1.0303
481×481	9.212e-7	1.6037	4.285e-5	1.0257	9.640e-5	0.8501

The absolute errors in the imaginary part of the complex-valued eikonal in three cases: at the single point (x, z) = (0, 1.0) km, along the line z = 1 km in the L_1 norm, and along z = 1 km in the L_2 norm.

T78 Leung et al.

single-valued solution becomes multivalued. In the region between -0.1 and 0.1 km at z=2.0 km, we even see as many as five arrivals. Figure 8 shows some comparisons of our PDE approach with the ray-tracing method. Similar to the observations made for the waveguide model, the ray-tracing solution is not uniformly sampled on the final arrival level; in particular, the first-arrival solution is poorly represented. However, our PDE approach can provide uniformly sampled solutions on any z-level. Figure 9 shows the imaginary part

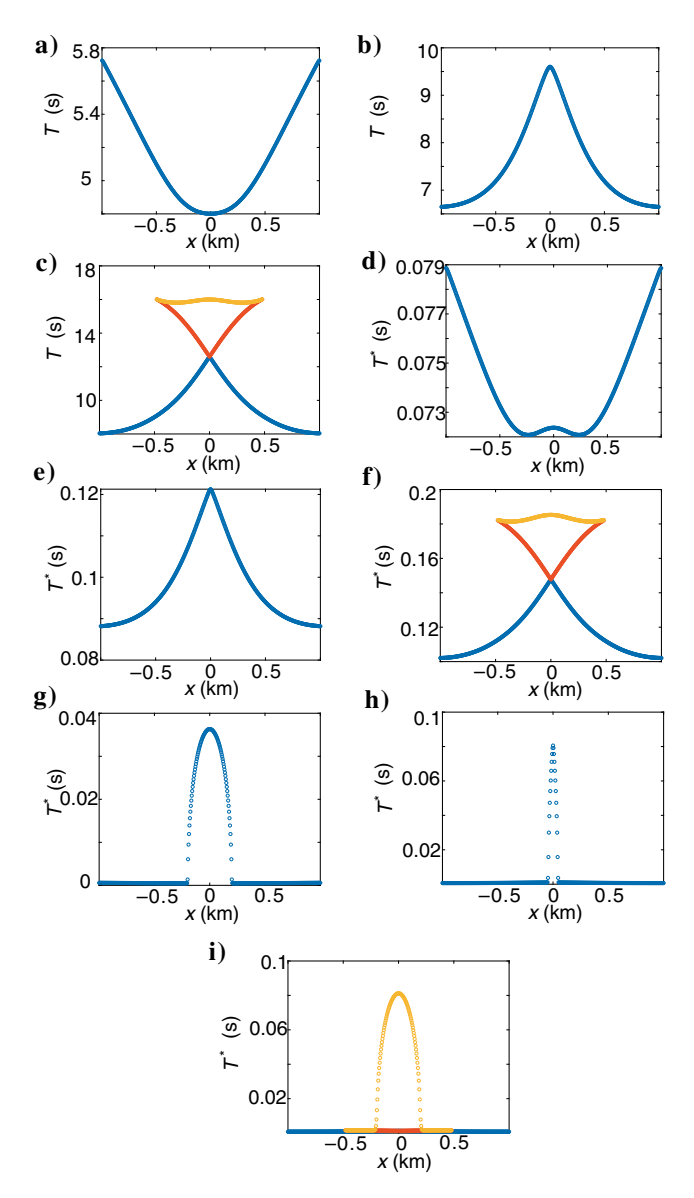


Figure 3. Waveguide model. The real part of the complex eikonal at (a) z=0.48 km, (b) z=0.96 km, and (c) z=1.6 km using a 480 × 480 grid. The imaginary part of the eikonal at (d) z=0.48 km, (e) z=0.96 km, and (f) z=1.6 km with the smooth model $Q=Q_1$. The imaginary part of the eikonal at (g) z=0.48 km, (h) z=0.96 km, and (i) z=1.6 km with the discontinuous model $Q=Q_2$. The error in the imaginary part of the eikonal for the third arrival (marked in yellow) at (x,z)=(0,1.6)km is given by 3.7947×10^{-16} for $Q=Q_1$ and 1.3317×10^{-5} for $Q=Q_2$, respectively. Blue curves: first arrival; cyan curves: second arrival; and yellow curves: third arrival.

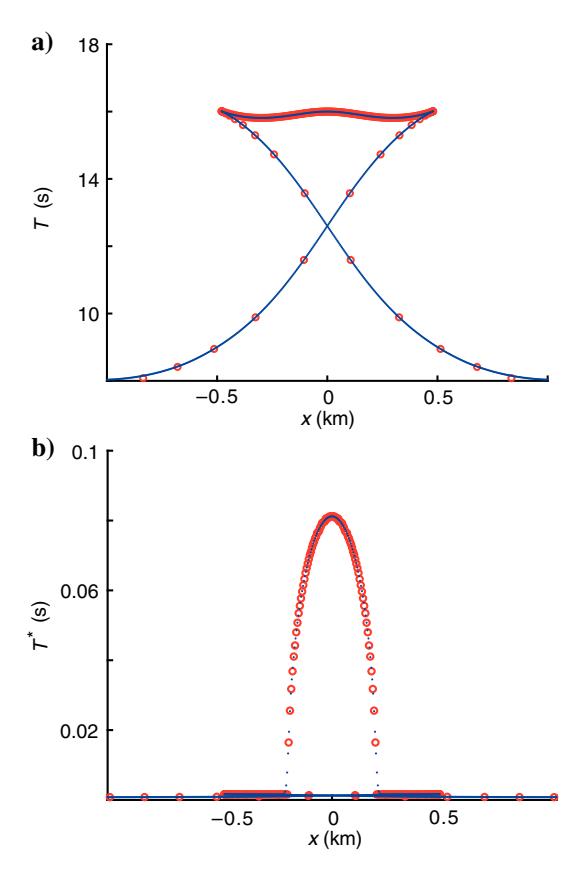


Figure 4. Waveguide model with $Q=Q_2$. Comparison of the complex-valued eikonal at $z=1.6\,\mathrm{km}$ for our method and the ray-tracing method. (a) The real part of the complex eikonal. (b) The imaginary part of the complex eikonal. The numerical solutions from our method are plotted using blue dots, and the ray-tracing solutions are shown using red circles.

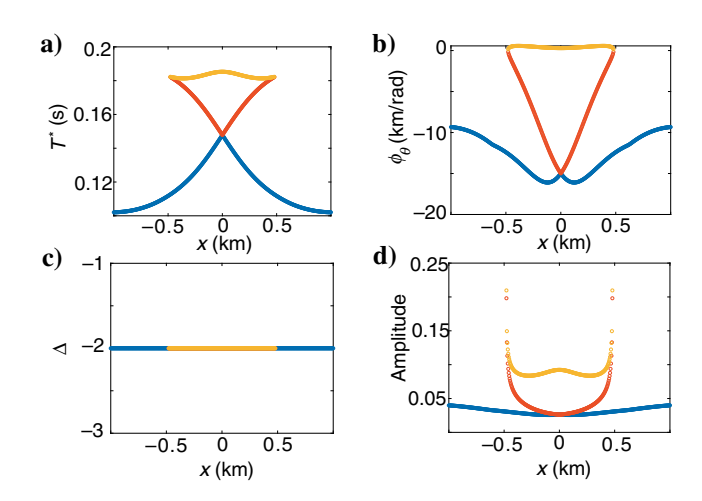


Figure 5. Waveguide model with $Q=Q_1$. The imaginary part T^* of the eikonal, the derivative of the level-set function ϕ_θ , the intermediate quantity Δ , and the amplitude A at z=1.6 km using a 481 \times 481 grid. Blue curves: first arrival; cyan curves: second arrival; and yellow curves: third arrival.

of the eikonal, $\phi_{\theta}, \; \Delta$ and also the amplitude at the final level z = 2.0 km. As the rays converge, the imaginary part of the eikonal also becomes multivalued. This shows that the proposed method obtains a uniformly spaced complex-valued eikonal in the region with diverging rays and the region with converging rays. This is beneficial for seismic imaging in complicated areas.

To demonstrate the effect of attenuation on seismic data, we model shot gathers in acoustic and viscoacoustic media. We assume that the multivalued real (or complex-valued) eikonal and amplitude functions consist of I(x, z) branches at each subsurface point (x, z),

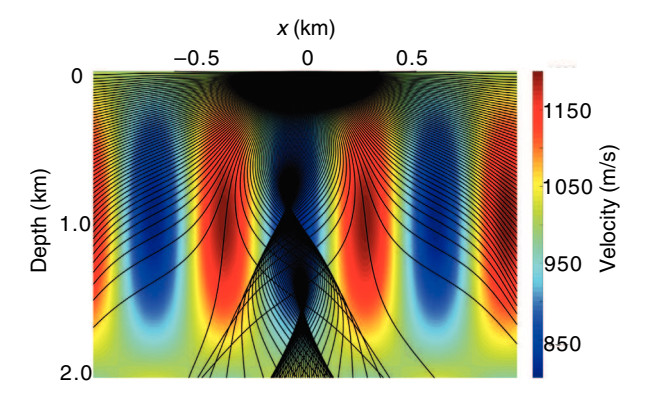


Figure 6. Sinusoidal model with rays.

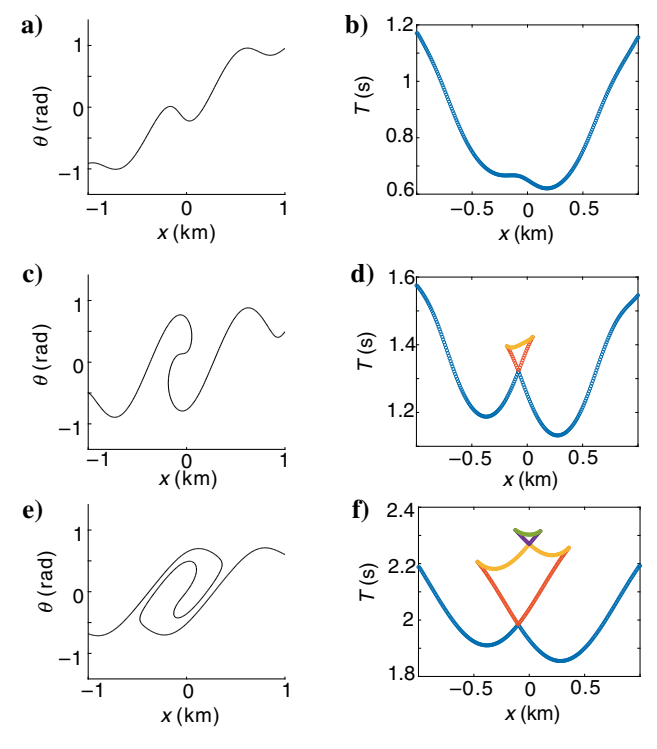


Figure 7. Sinusoidal model with $Q = Q_2$ using a 241 × 241 grid. The zero level set at (a) z = 0.6 km, (c) z = 1.2 km, and (e) z = 2.0 km. The real part of the complex-valued eikonal at (b) z = 0.6 km, (d) z = 1.2 km, and (f) z = 2.0 km. Blue curves: first arrival; cyan curves: second arrival; yellow curves: third arrival; pink curves: fourth arrival; and green curves: fifth arrival.

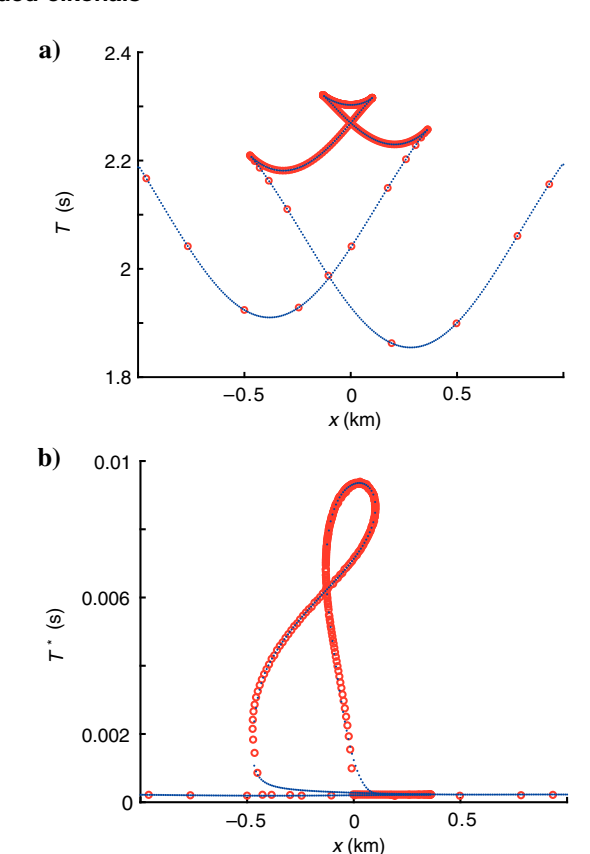


Figure 8. Sinusoidal model with $Q = Q_2$. Comparison of the complex-valued eikonal at z = 2 km for our method and the ray-tracing method. (a) The real part of the complex eikonal. (b) The imaginary part of the complex eikonal. The numerical solutions from our method are plotted using blue dots, and the ray-tracing solutions are shown using red circles.

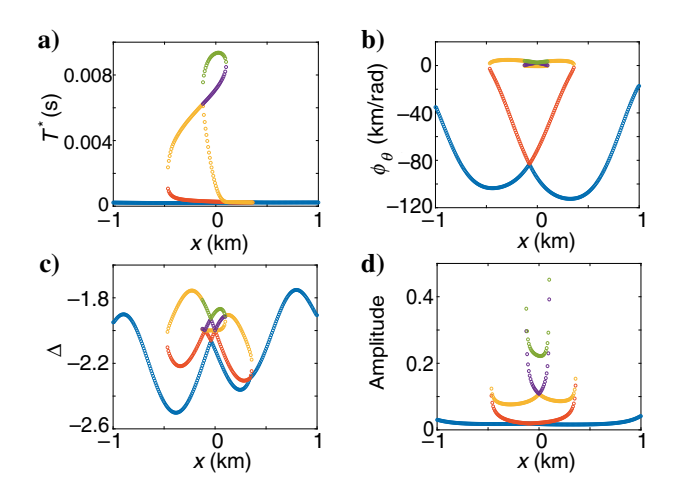


Figure 9. Sinusoidal model with $Q = Q_2$. The imaginary part T^* of the complex-valued eikonal, the derivative of the level-set function ϕ_{θ} , the intermediate quantity Δ , and the amplitude A at z=2.0 km. Blue curves: first arrival; cyan curves: second arrival; yellow curves: third arrival; pink curves: fourth arrival; and green curves: fifth arrival.

T80 Leung et al.

where I(x, z) is an integer varying from point to point. The shot gather is modeled using the multivalued eikonal and amplitude functions according to the following "truncated" formula:

$$d(x, z, \omega) = \sum_{i=1}^{I(x,z)} g(\omega) A_i(x, z) \exp(-i\omega t_i(x, z)), \qquad (26)$$

where ω is the angular frequency, $g(\omega)$ is the source wavelet, $d(x,z,\omega)$ is the shot gather in the frequency domain, $A_i(x,z)$ is the *i*th branch of the multivalued amplitude computed by the proposed Liouville method, and t_i is the *i*th branch of the multivalued eikonal. The frequency-domain shot gather $d(x,z,\omega)$ can be inverse Fourier transformed with respect to ω to obtain waves in the time domain.

We call equation 26 the truncated formula because we have ignored phase shifts of geometric optics across caustics (and/or cusps) in this formula. As a result, the resulting shot gathers experience a sharp change across caustics (and/or cusps), and such sharp changes are unrealistic. Nevertheless, in noncaustic but multivalued regions, our truncated construction reveals those interesting aspects of multivalued eikonals and resulting asymptotic solutions. We will treat phase shifts associated with multivalued eikonals more thoroughly in a future work.

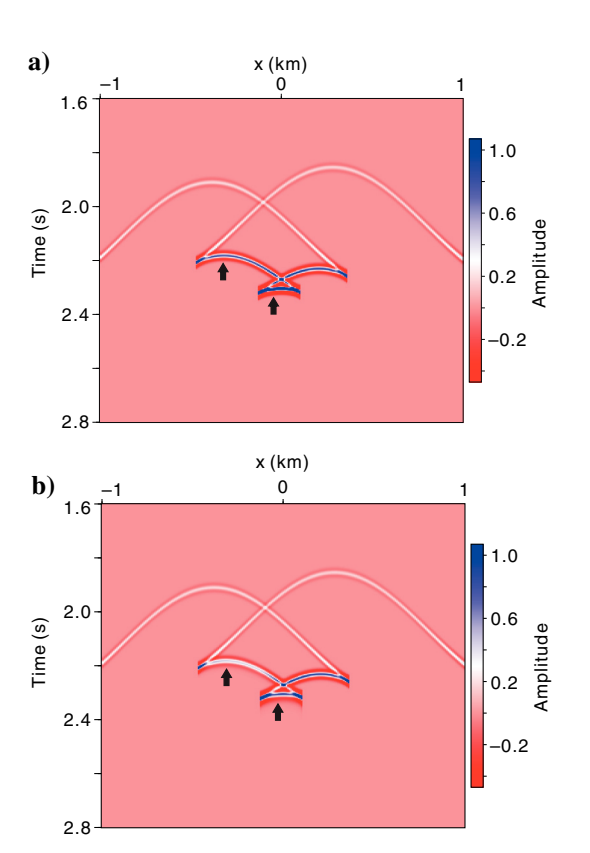


Figure 10. Comparison of shot gathers at z = 2.0 km for the acoustic medium and the viscoacoustic medium with $Q = Q_2$, where the reference velocity is the sinusoidal model. (a) The acoustic case and (b) the viscoacoustic case.

In an acoustic medium, t_i is T_i , the real part of the *i*th branch of the complex-valued eikonal. In a viscoacoustic medium, we define t_i using the Futterman's dispersion relation (Keers et al., 2001):

$$t_i(x,z) = T_i(x,z) - \frac{1}{\pi} T_i^*(x,z) \ln\left(\frac{\omega}{\omega_0}\right) - i \frac{T_i^*(x,z)}{2},$$
 (27)

where ω_0 is a reference angular frequency, which is usually a value close to the centroid of the amplitude spectrum.

We use a Ricker wavelet with a main frequency of 30 Hz. Figure 10 shows shot gathers obtained at z = 2.0 km for the two cases: Figure 10a for the acoustic medium defined by the sinusoidal velocity model, and Figure 10b for the viscoacoustic medium with the sinusoidal velocity as the reference velocity and the Q_2 function as the quality factor; these results illustrate that the seismic waves passing through the low Q area experience the frequency-dependent amplitude loss due to attenuation. We remark that although the shot gathers in both cases show unrealistic sharp changes across caustics due to the truncated formula 26, the resulting wavefields in noncaustic but multivalued regions do reveal the multivalued effects of eikonals. To demonstrate the difference of the two models in detail, we compare their traces and amplitude spectra at x = -0.0834 km, as shown in Figure 11. Note that the amplitude spectrum in Figure 11b is computed from the last wavelet in Figure 11a. Figure 11a shows that the seismic amplitude is greatly attenuated in the viscoacoustic medium, and the phase of wavelet also is changed due to the seismic attenuation. Figure 11b shows that the main frequency in the viscoacoustic medium is reduced, which further reduces the resolution of seismic data.

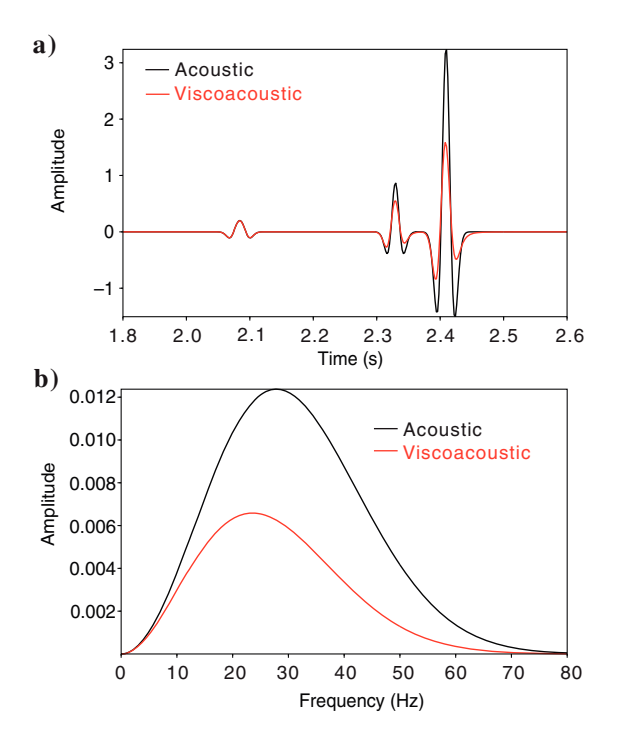


Figure 11. Comparison of traces for the sinusoidal model with $Q=Q_2$ at x=-0.0834 km and z=2.0 km. (a) Traces and (b) their amplitude spectra. Black lines: the acoustic medium and red lines: the viscoacoustic medium.

A synthetic gas-cloud model

In this example, we apply our method to a synthetic gas-cloud model. This synthetic model is constructed as follows. We first extract a velocity model from the BP 2007 tilted transversely isotropic velocity model, as shown in Figure 12a. We further construct a Q model according to the extracted velocity model: We fill the zone of low velocity in the shallow region with low Q values to simulate the gas cloud, and we set the Q value in other places to be 10,000 as shown in Figure 12b. The model dimension is 8 km in depth and 10 km laterally. The grid size is 10 m in the x- and z-axes so that the total number of grid points in physical space is 1001×801 in the velocity model. Numerically, we discretize phase space, the x- θ space, using a mesh of 1001 \times 1001 so that the mesh points in the x-direction align with the velocity model. To evolve the PDEs in the z-direction, the step size in z is determined by the stability condition of the numerical schemes for the PDEs, where the velocity and the Q model needed for the z-direction evolution will be obtained by linear interpolation in the z-direction.

To demonstrate that our proposed method can effectively capture multivalued solutions, we compute the multivalued solutions at a point source: (x, z) = (4.5, 0)km. The computational results are shown in Figures 13, 14, and 15. Figure 13 shows the evolution of the zero level set at various z-levels up to z = 7 km at the given point source, where the z-levels are given by 2.3873, 3.5810, 4.7746, and 7 km. We can clearly see that the zero level-set function overturns in phase space (the x- θ space) and develops very compli-

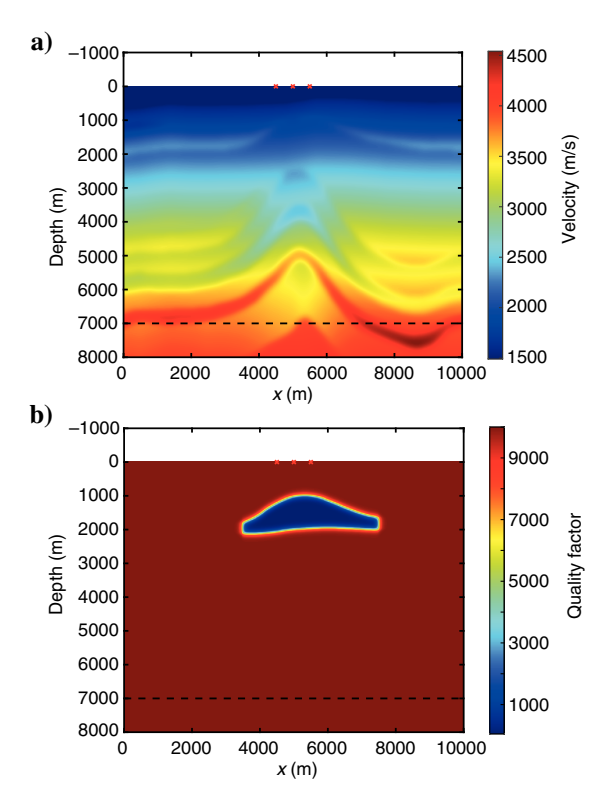


Figure 12. A synthetic gas-cloud model. (a) The velocity model and (b) the function Q defined on the domain $[0,10] \times [0,8]$ km with three different sources located at (x, z) = (4.5, 0) km, (x, z) = (5, 0) km, and (x, z) = (5.5, 0) km, where we will only show results for one source. Numerical solutions will be shown for the line z = 7 km.

cated structures. For each fixed x location, we can find more than one corresponding θ so that the level-set function vanishes. This implies that there are multiple arrivals initiated from the point source. Figure 14 shows magnification of the real part of the complex-valued eikonal for the given point source and its corresponding structure. The rays in the magnification area converge so that the eikonal becomes multivalued. Therefore, the results show that

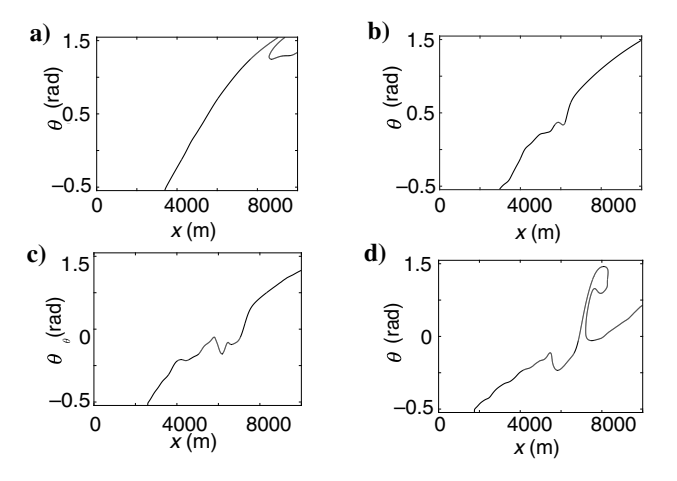


Figure 13. A synthetic gas-cloud model. The zero level set at (a) z = 2.3873 km, (b) z = 3.5810 km, (c) z = 4.7746 km, and (d) z = 7 km with the source located at (x, z) = (4.5, 0) km. Numerical solutions are computed on a mesh of 1001×1001 grid

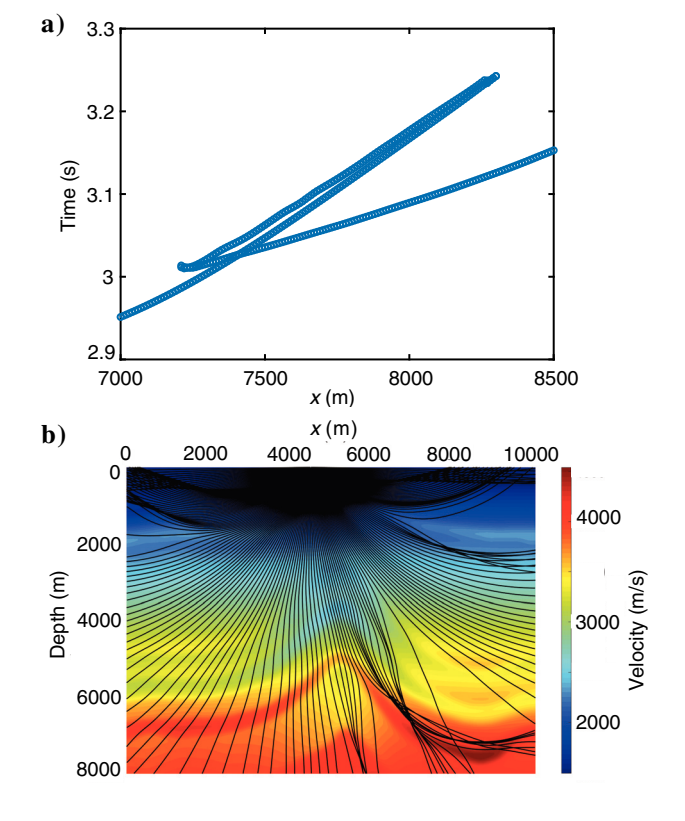


Figure 14. A synthetic gas-cloud model. (a) Magnification of the real part of the complex-valued eikonal at z = 7 km with the source located at (x, z) = (4.5, 0) km and (b) the related ray structure.

T82 Leung et al.

our proposed method is able to capture effectively multivalued eikonals. In Figure 15, we show the real part T and the imaginary part T^* of the eikonal, the amplitude function A, and also the intermediate quantity Δ , for the given point source.

Analogous to the sinusoidal model, we model shot gathers in the viscoacoustic medium and in the corresponding reference acoustic

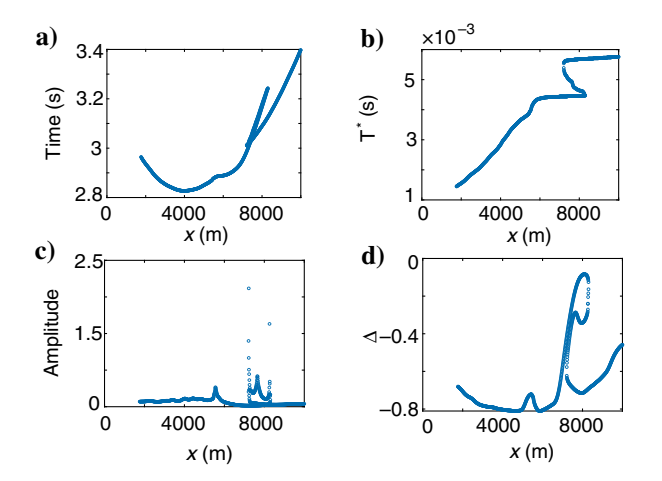


Figure 15. A synthetic gas-cloud model. The real part T and the imaginary part T^* of the complex-valued eikonal, the amplitude A, and the intermediate quantity Δ at z=7 km with the source located at (x,z)=(4.5,0)km.

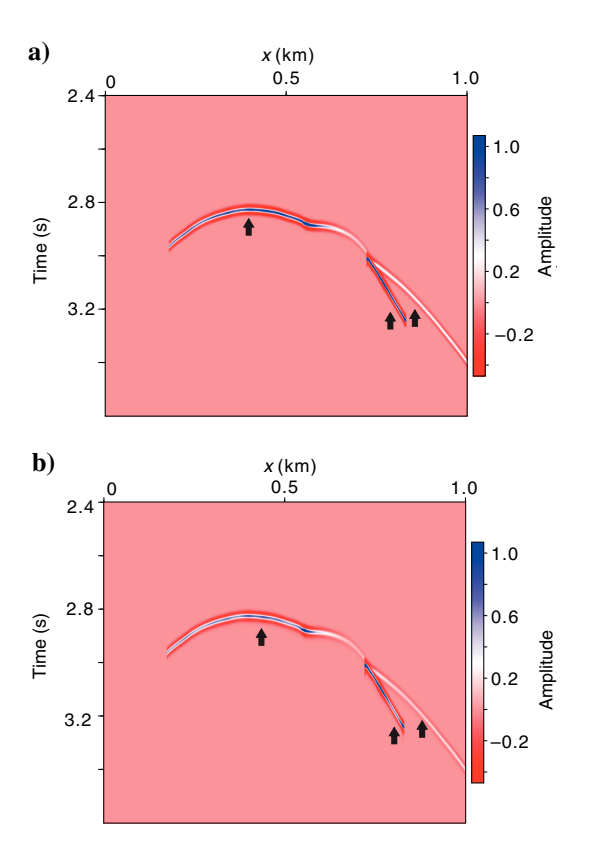


Figure 16. Comparison of shot gathers for the synthetic gas-cloud model at z = 7.0 km. (a) The acoustic case and (b) the viscoacoustic case. The source is located at (x, z) = (4.5, 0) km.

medium to demonstrate the effect of attenuation on seismic data. We use a Ricker wavelet with a main frequency of 30 Hz. Figure 16 shows a shot gather obtained at $z=7.0\,\mathrm{km}$ for the source located at $(x,z)=(4.5,0)\,\mathrm{km}$. The comparison of shot gathers shows that the seismic wave passing through the low Q area suffers from amplitude attenuation. Their traces and amplitude spectra at $x=0.5\,\mathrm{km}$ are compared in Figure 17. Figure 17a shows that the amplitude of seismic waves is greatly attenuated, and the phase of wavelet also is changed due to seismic attenuation. Figure 17b shows that the main frequency in the viscoacoustic medium is reduced, which further reduces the resolution of seismic data. We remark again that although the shot gathers in both cases show unrealistic sharp changes across caustics due to the truncated formula 26, the resulting wavefields in noncaustic but multivalued regions do reveal the multivalued effects of eikonals.

DISCUSSION

Lagrangian versus Eulerian formulation

Lagrangian ray-tracing methods and Eulerian methods have their advantages and disadvantages, depending on what is needed in specific applications. As discussed and illustrated in Leung et al. (2007) for Gaussian beams, a Lagrangian ray-tracing method is able to control how the initial values of rays, such as source locations and takeoff angles, are distributed, but it is not able to control how arrival locations and arrival angles of rays are distributed. In contrast, an Eulerian method as proposed here is able to control how arrival locations and arrival angles are distributed, but it is not able to control how initial source locations and takeoff angles are distributed. Therefore, one may choose which method to use according to the specific application in hand.

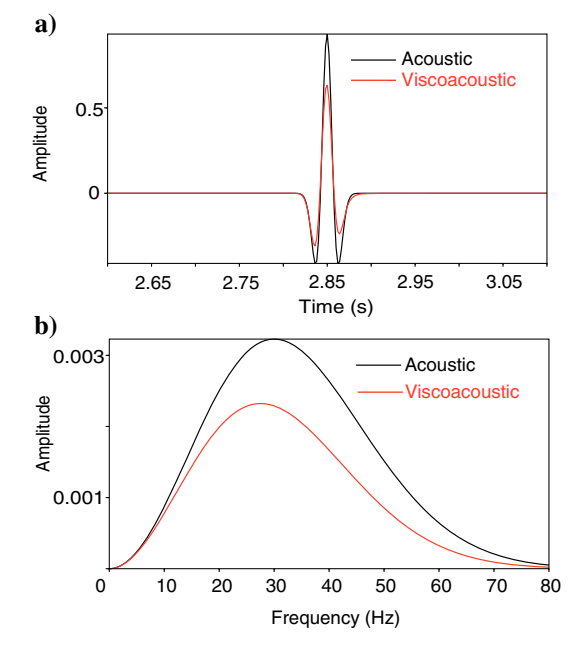


Figure 17. Comparison of traces for the synthetic gas-cloud model at x = 0.5 km and z = 7.0 km. (a) Traces and (b) their amplitude spectra. Black lines: the acoustic case and red lines: the viscoacoustic case. The source is located at (x, z) = (4.5, 0) km.

The subhorizontal condition

We have imposed the subhorizontal condition in our computational formulation to expedite the development and implementation of our algorithm; consequently, we are only able to capture one-way wave propagation in the depth direction. This condition can be removed by incurring some additional cost. Essentially, one may use the formulation developed in Qian et al. (2003) to compute all the multivalued ingredients in the entire phase space, so that overturning and steepdipping waves can be captured faithfully. This work is ongoing.

Anisotropy

Our Liouville formulation is able to compute naturally multivalued eikonals in nonattenuating anisotropic wave propagation, as illustrated in Qian and Leung (2004) and Qian et al. (2003), where the Liouville equations are developed for computing multivalued eikonals of three wave modes (qP, qSV, and qSH). It is necessary to further develop our framework to compute multivalued eikonals in attenuating anisotropic media so that complex eikonals of the three wave modes in viscoelastic anisotropic media can be computed efficiently; this work is ongoing.

CONCLUSION

We have presented Liouville PDE methods for computing complex-valued eikonals in real space in the multivalued sense in attenuating media. The proposed method is capable of computing complexvalued eikonals by providing the real and imaginary parts of the eikonal function in real space in the multivalued sense on regular meshes. This has been achieved by solving novel paraxial Liouville PDEs in real phase space, leading to efficient Eulerian PDE methods for multivalued solutions. We also are able to compute multivalued amplitudes when the quality factor satisfies certain conditions in a viscoacoustic medium. Numerical examples, including a synthetic gas-cloud model, illustrated that the proposed methods yield highly accurate complex-valued eikonals in the multivalued sense. The proposed methods can be used for migration and tomography in attenuating media.

ACKNOWLEDGMENTS

Leung is partially supported by the Hong Kong RGC (grant no. 16302819). Hu appreciates the financial support from the National Natural Science Foundation of China (grant nos. 42074166 and 42074163). Qian is partially supported by the National Science Foundation (grant nos. 1614566 and 2012046). We thank J. Etgen, C. Torres-Verdin, S. Hestholm, S. Gray, B. Zhou, and two anonymous reviewers for helpful comments and suggestions.

DATA AND MATERIALS AVAILABILITY

Data associated with this research are available and can be obtained by contacting the corresponding author.

REFERENCES

Aki, K., and P. Richards, 1980, Quantitative seismology: Freeman and Co. Benamou, J.-D., 1999, Direct solution of multi-valued phase-space solutions for Hamilton-Jacobi equations: Communications on Pure and Applied Mathematics, **52**, 1443–1475, doi: 10.1002/(SICI)1097-0312(199911) 52:11<1443::AID-CPA3>3.0.CO;2-Y.

- Blanch, J. O., and J. O. A. Robertsson, 1997, A modified Lax-Wendroff correction for wave propagation in media described by Zener elements: Geophysical Journal International, 131, 381–386, doi: 10.1111/j.1365-
- Blanch, J. O., J. O. A. Robertsson, and W. W. Symes, 1995, Modeling of a constant Q: Methodology and algorithm for an efficient and optimally inexpensive viscoelastic technique: Geophysics, 60, 176–184, doi: 10 1190/1 144374
- Carcione, J. M., 1999, Staggered mesh for the anisotropic and viscoelastic
- wave equation: Geophysics, **64**, 1863–1866, doi: 10.1190/1.1444692. Carcione, J. M., 2009, Theory and modeling of constant-Q P- and S-waves using fractional time derivatives: Geophysics, 74, no. 1, T1-T11, doi: 10
- Carcione, J. M., 2015, Wave fields in real media: Theory and numerical simulation of wave propagation in anisotropic, anelastic, porous and electromagnetic media: Handbook of geophysical exploration, 3rd ed.: Elsevier.
- Carcione, J. M., F. Cavallini, F. Mainardi, and A. Hanyga, 2002, Time domain seismic modeling of constant-Q wave propagation using fractional derivatives: Pure and Applied Geophysics, **159**, 1719–1736, doi: 10.1007/
- Červený, V., I. A. Molotkov, and I. Psencik, 1977, Ray method in seismology: Univerzita Karlova Press.
- ogy: Univerzita Kariova Press.

 Engquist, B., O. Runborg, and A.-K. Tornberg, 2002, High frequency wave propagation by the segment projection method: Journal of Computational Physics, 178, 373–390, doi: 10.1006/jcph.2002.7033.

 Fomel, S., and J. Sethian, 2002, Fast phase space computation of multiple
- arrivals: Proceedings of the National Academy of Sciences of the United States of America, **99**, 7329–7334, doi: 10.1073/pnas.102476599.
- Gajewski, D., and I. Pšenčik, 1992, Vector wavefields for weakly attenuating anisotropic media by the ray method: Geophysics, 57, 27-38, doi: 10 1190/1.1443186
- Goldstein, H., 1950, Classical mechanics: Addison-Wesley Publishing Company.

 Gray, S., 2005, Gaussian beam migration of common shot records:
- Geophysics, 70, no. 4, S71-S77, doi: 10.1190/1.1988186
- Gray, S., and W. May, 1994, Kirchhoff migration using eikonal equation traveltimes: Geophysics, 59, 810-817, doi: 10.1190/1.1443639
- Hanyga, A., and M. Seredyńska, 2000, Ray tracing in elastic and viscoelastic media: Pure and Applied Geophysics, 157, 679–717, doi: 10.1007/
- Hao, Q., and T. Alkhalifah, 2017, An acoustic eikonal equation for attenuating transversely isotropic media with a vertical symmetry axis: Geophysics, **82**, no. 1, C9–C20, doi: 10.1190/geo2016-0160.1.
- Hill, N., 2001, Prestack Gaussian-beam depth migration: Geophysics, 66, 1240–1250, doi: 10.1190/1.1487071.
- Hu, J., J. Qian, J. Song, M. Ouyang, J. Cao, and S. Leung, 2021, Eulerian partial-differential equation methods for complex-valued eikonals in attenuating media: Geophysics, **86**, no. 4, T179–T192, doi: 10.1190/
- Hu, J. T., P. Wang, J. X. Cao, H. Z. Wang, and X. J. Wang, 2018, Frequency dependent complex traveltime computation in TI media with weak attenuation using Fermat's principle based fast marching: 88th Annual International Meeting, SEG, Expanded Abstracts, 4040–4044, doi: 10 .1190/segam2018-299
- Huang, X., and S. Greenhalgh, 2018, Linearized formulations and approximate solutions for the complex eikonal equation in orthorhombic media and applications of complex seismic traveltime: Geophysics, 83, no. 3, C115-C136, doi: 10.1190/geo2017-0620.1.
- Huang, X., J. Sun, and S. Greenhalgh, 2018, On the solution of the complex eikonal equation in acoustic VTI media: A perturbation plus optimization scheme: Geophysical Journal International, 214, 907–932, doi: 10.1093/
- Jiang, G. S., and D. Peng, 2000, Weighted ENO schemes for Hamilton-Ja-cobi equations: SIAM Journal on Scientific Computing, 21, 2126–2143,
- Keers, H., D. W. Vasco, and L. R. Johnson, 2001, Viscoacoustic crosswell imaging using asymptotic waveforms: Geophysics, 66, 861–870, doi: 10
- Klimeš, M., and L. Klimeš, 2011, Perturbation expansions of complex-valued traveltime along real-valued reference rays: Geophysical Journal International, **186**, 751–759, doi: 10.1111/j.1365-246X.2011.05054.x.
- Leung, S., J. Qian, and R. Burridge, 2007, Eulerian Gaussian beams for high frequency wave propagation: Geophysics, 72, no. 5, SM61-SM76, doi:
- Leung, S., J. Qian, and S. J. Osher, 2004, A level set method for three dimensional paraxial geometrical optics with multiple sources: Communications in Mathematical Sciences, **2**, 643–672, doi: 10.4310/CMS.2004.v2.n4.a5.
- Li, X., B. Zhou, C. Bai, and J. Wu, 2020, Seismic complex ray tracing in 2D/ 3D viscoelastic anisotropic media by a modified shortest-path method: Geophysics, **85**, no. 6, T331–T342, doi: 10.1190/geo2020-0113.1. Lions, P. L., 1982, Generalized solutions of Hamilton-Jacobi equations:
- Pitman Advanced Publishing Program.

T84 Leung et al.

Liu, Z., and N. Bleistein, 1995, Migration velocity analysis: Theory and an iterative algorithm: Geophysics, 60, 142–153, doi: 10.1190/1.1443741.
 Operto, S., S. Xu, and G. Lambare, 2000, Can we image quantitatively com-

- plex models with rays: Geophysics, 65, 1223-1238, doi: 10.1190/1
- Osher, S., L.-T. Cheng, M. Kang, H. Shim, and Y.-H. Tsai, 2002, Geometrical optics in a phase space based level set and Eulerian framework: Journal of Computational Physics, **179**, 622–648, doi: 10.1006/jcph.2002.7080.
 Osher, S. J., and C. W. Shu, 1991, High-order essentially nonoscillatory schemes for Hamilton-Jacobi equations: SIAM Journal on Numerical Applying **28**, 027, 022, doi: 10.1137/0739040
- Analysis, 28, 907-922, doi: 10.1137/0728049
- Peng, D., B. Merriman, S. Osher, H. K. Zhao, and M. Kang, 1999, A PDEbased fast local level set method: Journal of Computational Physics, 155, 410-438, doi: 10.1006/jcph.1999.6345.
- Pereyra, V., 1992, Two-point ray tracing in general 3-D media: Geophysical Prospecting, 40, 267–287, doi: 10.1111/j.1365-2478.1992.tb00375.x. Qian, J., L.-T. Cheng, and S. J. Osher, 2003, A level set based Eulerian ap-
- proach for anisotropic wave propagations: Wave Motion, **37**, 365–379, doi: 10.1016/S0165-2125(02)00101-4.
- Qian, J., and S. Leung, 2004, A level set method for paraxial multivalued traveltimes: Journal of Computational Physics, 197, 711–736, doi: 10 .1016/j.jcp.2003.12.017
- Qian, J., and S. Leung, 2006, A local level set method for paraxial multivalued geometric optics: SIAM Journal on Scientific Computing, 28, 206–223, doi: 10.1137/030601673.

 Qian, J., and W. W. Symes, 2002, An adaptive finite difference method for travial to the control of the control of
- eltime and amplitude: Geophysics, **67**, 167–176, doi: 10.1190/1.1451472. Robertsson, J. O. A., J. O. Blanch, and W. W. Symes, 1994, Viscoelastic finite-difference modeling: Geophysics, **59**, 1444–1456, doi: 10.1190/1
- Symes, W. W., 1998, A slowness matching finite difference method for traveltimes beyond transmission caustics: 68th Annual International Meeting, SEG, Expanded Abstracts, 1945–1948, doi: 10.1190/1
- Symes, W. W., and J. Qian, 2003, A slowness matching Eulerian method for multivalued solutions of eikonal equations: Journal of Scientific Computing, 19, 501-526, doi: 10.1023/A:1025380731197
- van Trier, J., and W. W. Symes, 1991, Upwind finite-difference calculation of traveltimes: Geophysics, **56**, 812–821, doi: 10.1190/1.1443099.
- Vavryčuk, V., 2008a, Real ray tracings in anisotropic viscoelastic media: Geophysical Journal International, 175, 617–626, doi: 10.1111/j.1365-246X.2008.03898.x.

- Vavryčuk, V., 2008b, Velocity, attenuation and quality factor in anisotropic viscoelastic media: A perturbation approach: Geophysics, 73, no. 5, D63-D73, doi: 10.1190/1.2921778.
- Vavryčuk, V., 2012, On numerically solving the complex eikonal equation using real ray-tracing methods: A comparison with the exact analytical solution: Geophysics, 77, no. 4, T109–T116, doi: 10.1190/geo2011-0431.
 Vinje, V., E. Iversen, and H. Gjystdal, 1993, Traveltime and amplitude es-
- timation using wavefront construction: Geophysics, 58, 1157-1166, doi: 10.1190/1.1443499
- White, B. S., 1984. The stochastic caustic: SIAM Journal on Applied Mathematics, 44, 127–149, doi: 10.1137/0144010.
- Xie, Y., J. Sun, Y. Zhang, and J. Zhou, 2015, Compensating for visco-acoustic effects in TTI reverse time migration: 85th Annual International Meeting, SEG, Expanded Abstracts, 3996–4001, doi: 10.1190/segam2015-
- Xie, Y., K. Xin, J. Sun, and C. Notfors, 2009, 3D prestack depth migration with compensation for frequency dependent absorption and dispersion: 79th Annual International Meeting, SEG, Expanded Abstracts, 2919–
- Xin, K. F., Y. He, Y. Xie, W. Q. Xu, and M. Wang, 2014, Robust Q tomographic inversion through adaptive extraction of spectral features: 84th Annual International Meeting, SEG, Expanded Abstracts, 3726–3730, doi: 10.1190/segam2014-0421.1.
- You, G., and S. Leung, 2018, Eulerian based interpolation schemes for flow map construction and line integral computation with applications to coherent structures extraction: Journal of Scientific Computing, **74**, 70–96, doi: 10.1007/s10915-017-0424-9.
- You, G., and S. Leung, 2020, Fast construction of forward flow maps using Eulerian based interpolation schemes: Journal of Scientific Computing, 82, 1–31, doi: 10.1007/s10915-020-01141-z.
- You, G., T. Wong, and S. Leung, 2017, Eulerian methods for visualizing continuous dynamical systems using Lyapunov exponents: SIAM Journal on Scientific Computing, 39, A415–A437, doi: 10.1137/
- Zhang, L., 1993, Imaging by the wavefront propagation method: Ph.D. thesis, Stanford University
- Zhang, Y., P. Zhang, and H. Zhang, 2010, Compensating for visco-acoustic effects in reverse time migration: 80th Annual International Meeting, SEG, Expanded Abstracts, 3160–3164, doi: 10.1190/1.3513503.

Biographies and photographs of the authors are not available.